

The cosmic X-ray background: abundance and evolution of hidden black holes

R. Gilli

INAF – Osservatorio Astronomico di Bologna, Via Ranzani 1, I-40127 Bologna, Italy
e-mail: roberto.gilli@oabo.inaf.it

Abstract. The growth of supermassive black holes across cosmic time leaves a radiative imprint recorded in the X-ray background (XRB). The XRB spectral shape suggests that a large population of distant, hidden nuclei must exist, which are now being revealed at higher and higher redshifts by the deepest surveys performed by Chandra and XMM. Our current understanding of the XRB emission in terms of AGN population synthesis models is here reviewed, and the evolutionary path of nuclear accretion and obscuration, as emerging from the major X-ray surveys, is investigated. The role of galaxy merging versus secular processes in triggering nuclear activity is also discussed in the framework of recent galaxy/black hole co-evolutionary scenarios. Finally, the limits of current instrumentation in the detection of the most obscured and distant black holes are discussed and some possible directions to overcome these limits are presented.

Key words. X-rays: galaxies – Galaxies: active – X-rays: diffuse background

1. Introduction

Fifty years of technological progresses and scientific investigations since its discovery, have revealed the main essence of the cosmic X-ray background (XRB), the diffuse X-ray glow pervading the sky discovered by Giacconi et al. in 1962 in the first X-ray astronomy experiment. From that first rocket flight to the deepest observations now performed with Chandra and XMM, X-ray surveys gained ten orders of magnitude in sensitivity. This progress showed that, at energies below 10 keV, the XRB glow is resolved into hundreds of millions of individual X-ray sources distributed across the whole Universe: most of them are accreting supermassive black holes shining as Active Galactic Nuclei (AGN) at different epochs. In

the center of the deepest X-ray field to date, the 4Ms Chandra Deep Field South (4Ms CDFS; Xue et al. 2011), an AGN surface density of $\sim 10^4 \text{deg}^{-2}$ is observed down to $f_{2-8\text{keV}} \sim 5 \times 10^{-17} \text{erg cm}^{-2} \text{s}^{-1}$, whose integrated emission can virtually account for most of, if not all, the XRB surface brightness below 10 keV (Xue et al., 2011; Moretti et al., 2012). At higher energies, however, in the 20-40 keV energy range, where the XRB spectrum peaks, only a tiny fraction of its emission has been resolved into individual sources, mainly because of the limitations of high-energy instrumentation. A large portion of the XRB emission at 30 keV is expected to be produced by the same sources observed in the deep X-ray surveys like the 4Ms CDFS, just by simply extrapolating their spectra to higher energies. However, the very shape of the XRB spectrum calls for an ad-

Send offprint requests to: R.Gilli

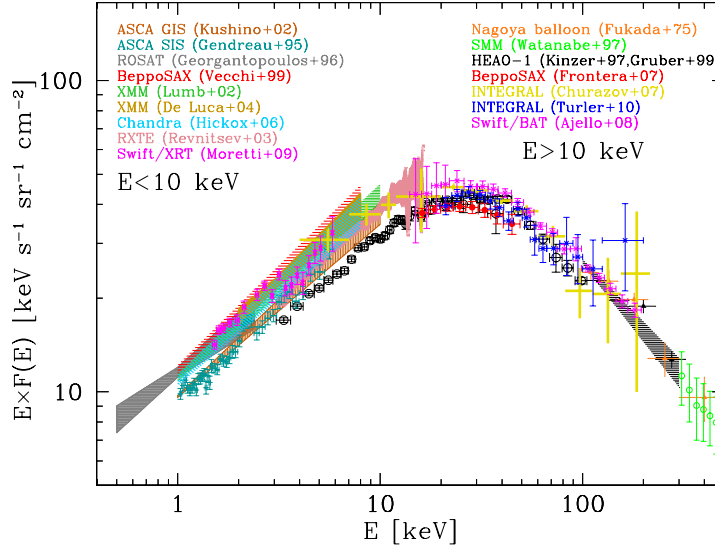


Fig. 1. Compilation of the measurements of the cosmic X-ray background spectrum in the 0.5 - 400 keV energy range. Datapoints with different colors come from different combinations of missions and instruments as labeled and referenced (*left labels*: $E < 10$ keV; *right labels*: $E > 10$ keV).

ditional large population of heavily obscured, Compton-thick AGN (hereafter CT AGN, $N_{\text{H}} \geq 10^{24} \text{cm}^{-2}$) poorly sampled by most surveys at $E < 10$ keV. Despite several efforts, the cosmological evolution and luminosity function of CT objects remain essentially unknown and have to be postulated by AGN population synthesis models trying to explain the XRB broad band spectrum (see next Section). Heavily hidden black holes are then likely the key and still missing ingredient to get a complete understanding of the cosmic XRB, keeping it one of the most fascinating and challenging topics in high-energy astrophysics.

2. The synthesis of the X-ray background: Compton-thick AGN and the “missing” fraction

The broad band, 0.5-400 keV XRB spectrum has a characteristic shape peaking at $E \sim 30$ keV. Below 10 keV it can be approximated by a power law with $\Gamma \sim 1.4$, i.e. it is harder than the average spectrum of bright, unobscured QSOs. A compilation of XRB measurements includ-

ing the most recent results by Chandra and XMM at $E < 10$ keV, and BeppoSAX, Swift and INTEGRAL at $E > 10$, keV is shown in Fig.1. The various measurements generally agree on the spectral shape, but possess significant scatter, at the 20-30% level, in their absolute normalization (in general, most of the recent XRB measures were found to be higher than the classic value measured by HEAO-1 in the 80s). The origin of this scatter is still debated. Part of it, but limited to the measures performed in pencil beam surveys, could arise from cosmic variance. Another source of uncertainty could be the stray-light which is entering an X-ray telescope field of view if not properly modeled (Moretti et al., 2012). Finally, $>10\%$ calibration uncertainties have been observed among different instruments on board different, or even the same, missions (Tsujimoto et al., 2011), which could explain another part of the scatter. It is then fair to conclude that the XRB absolute flux is known with a $\sim 20\%$ systematic uncertainty.

In 1989 Setti & Woltjer first proposed that the hard XRB spectrum could be explained

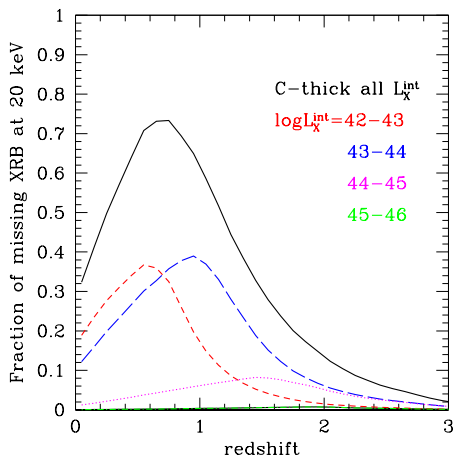


Fig. 2. Fraction of the XRB emission at 20 keV produced by CT AGN at different redshifts in the Gilli et al. (2007) model. The emission from the whole CT population (black line) is splitted into four bins of intrinsic 2-10 keV luminosity L_x^{int} (color curves): most of the “missing” XRB is expected to be produced by objects with $L_x^{int} < 10^{44}$ erg s $^{-1}$ and $z < 1$.

by the superposition of AGN spectra with different absorption degrees. This prompted the flourishing of a series of AGN population synthesis models with an increasing degree of complexity, including: detailed spectra and absorption distributions (Madau et al., 1994; Comastri et al., 1995); a careful treatment of Compton scattering in heavily obscured sources (Wilman & Fabian, 1999; Pompilio et al., 2000); the inclusion of iron features (Gilli et al., 1999); evolution of the obscured AGN fraction with luminosity (Ueda et al., 2003) and redshift (La Franca et al., 2005; Ballantyne et al., 2006; Treister et al., 2009); dispersion in the AGN primary spectral slopes (Gilli et al., 2007); exploration of the full parameter space (e.g. reflection fraction vs CT abundance; Treister et al. 2009; Akylas et al. 2012). These works suggested that 10-30% of the XRB emission at 30 keV, depending on the model assumptions and on the adopted XRB normalization, is produced by CT AGN. Gilli et al. (2007) splitted the population of CT AGN into a pair of evenly populated categories of transmission-dominated ($N_H \sim 10^{24}$ cm $^{-2}$) and reflection dominated ($N_H > 10^{25}$ cm $^{-2}$) objects,

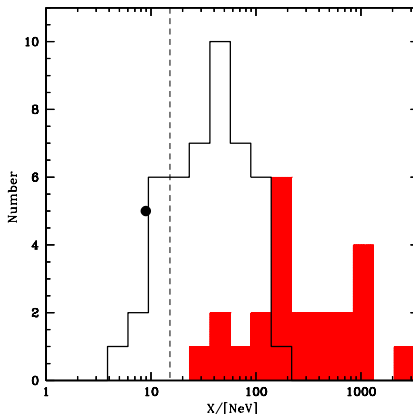


Fig. 3. The distribution of the observed 2-10 keV to [Ne V] luminosity ratio (X/NeV) for the [Ne V]-selected Type-2 AGN in COSMOS. Filled and empty histograms refer to X-ray detections and upper limits, respectively. The filled dot ($X/NeV \sim 9$, arbitrary position on the y-axis) is derived by stacking X-ray undetected sources. The vertical dashed line marks the threshold to select candidate CT AGN ($X/NeV < 15$). From Mignoli et al. (2013).

and built a self-consistent synthesis model in which CT AGN are as abundant as less absorbed objects. However, this result is far from being conclusive: as Comastri et al. (2008) showed, varying the number of reflection-dominated objects by a factor of four was still consistent with the XRB spectrum. This suggests that the XRB spectrum has limited constraining power and that an accurate estimate of the abundance of CT AGN can only be determined by *direct* object selection.

In Fig.2 it is shown the fraction of the XRB emission at 20 keV produced by CT AGN (the so-called “missing” XRB) as a function of their redshift in the Gilli et al. (2007) model. Most of the “missing” XRB is expected to be produced by Seyfert-like CT objects at $z \sim 0.7$ (i.e. with intrinsic 2-10 keV luminosity $L_x^{int} < 10^{44}$ erg s $^{-1}$). A direct sampling of this very population is therefore highly desirable, and it has been recently attempted by Mignoli et al. (2013) who used the [Ne V]3426Å emission line to pinpoint narrow line (type-2) AGN among the ~ 7400 galaxies at $0.65 < z < 1.2$ in the

zCOSMOS spectroscopic survey (Lilly et al., 2007). Seventytwo type-2 AGN with Seyfert-like luminosities and average redshift 0.9 were found in the survey area covered by Chandra ($\sim 0.9\text{deg}^2$, the C-COSMOS survey, Elvis et al. 2009): among them, 46 objects with X-ray to NeV ratio lower than 100 were accounted as heavily obscured AGN, including 9 CT candidates with $X/\text{NeV} < 15$. The distribution of the X/NeV ratios for this sample is shown in Fig.3: by stacking the X-ray undetected sources we derived an average X/NeV ratio of 9, which points towards a CT fraction in the whole type-2 sample of $\approx 41\%$ (see the detailed simulations in Mignoli et al. 2013), in line with the 50% fraction assumed in the Gilli et al. (2007) model. This measurement will be further refined by the forthcoming 2.8Ms Chandra COSMOS-Legacy data (PI F. Civano).

3. Evolution of nuclear obscuration and triggering mechanisms

While an overall self-consistent picture is emerging on the CT AGN population from the previous estimates, it is recalled that any estimate of nuclear absorption based on the comparison between some proxy of the intrinsic power (e.g. high-ionization lines such as [O III] or [Ne V], or mid-infrared luminosity) and the observed X-ray emission is highly uncertain, and in turn affects the estimate of the space density of CT AGN (see e.g. Fiore et al. 2009; Vignali et al. 2010; Georgantopoulos et al. 2011; Alexander et al. 2011). The only unambiguous way to select bona-fide CT AGN is through X-ray spectroscopy, and deep X-ray surveys are key to this. As an example, several CT AGN, up to $z \sim 5$, have been reported in the CDFS based either on Chandra or XMM data (Norman et al., 2002; Tozzi et al., 2006; Georgantopoulos et al., 2007; Comastri et al., 2011; Feruglio et al., 2011; Gilli et al., 2011). These numbers are too small to compute their space density and evolution, and this situation is unlike to change unless new X-ray facilities become available (see next Section). Nonetheless, X-ray spectroscopy in the deep Chandra and XMM surveys is shedding light on another very controversial issue, i.e. the

evolution history of Compton-thin obscuration. Several works in the past years claimed that the fraction of obscured nuclei increases with redshift (La Franca et al., 2005; Hasinger, 2008; Treister et al., 2009). This relation was not found by others (Ueda et al., 2003; Gilli et al., 2007), leading Gilli et al. (2010) to propose that strong selection effects were producing most of it. X-ray spectroscopy in the Chandra/XMM deep fields is shedding new light on this issue. Iwasawa et al. (2012) analyzed the XMM spectra of 46 AGN at $z > 1.7$ in the XMM-CDFS and found that the fraction of luminous ($L_{2-10}^{\text{rest}} \geq 10^{44} \text{erg s}^{-1}$) obscured QSOs was significantly higher than that observed in the local Universe by Burlon et al. (2011), and that selection biases could not explain this difference. Based on the Chandra spectra of a sample of 34 AGN at $z > 3$ in the 4Ms CDFS, Vito et al. (2013) found that the increase of the obscured AGN fraction with redshift was less significant or even absent at lower luminosities. This behaviour has an interesting qualitative interpretation in a scenario involving two modes of accretion/obscuration, which could mirror the two modes of star formation (bursting vs secular/main sequence) observed in the galaxy population (Elbaz et al., 2011; Rodighiero et al., 2011). Indeed, bright QSOs are preferentially found in starburst systems, while lower-luminosity objects are preferentially seen in main sequence galaxies (Rovilos et al., 2012). Furthermore, the fraction of AGN and star forming systems in mergers increases with their bolometric luminosity and “starburstiness”, respectively (Treister et al., 2012; Kartaltepe et al., 2012). Based on all this evidence, Iwasawa et al. (2012) suggested that the luminosity-dependent increase of the obscured AGN fraction with redshift could be related to the higher merger rate and gas fraction f_{gas} in galaxies at high redshift. As often postulated (e.g. Hopkins et al. 2008), mergers/interactions could trigger both powerful nuclear accretion and a starburst with compact and chaotic geometry, installing an evolutionary sequence in which, after an initial obscured phase, the black holes quickly (0.01-0.1 Gyr) clears its close environment and shines as an unobscured QSO. The higher

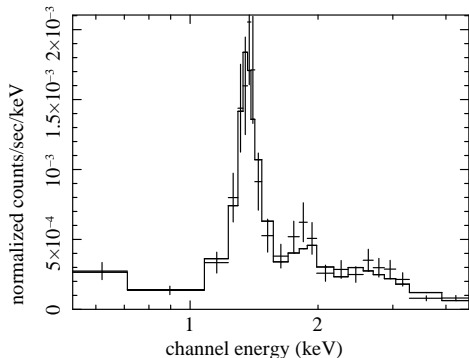


Fig. 4. Simulated WFXT spectrum of CDFS-202, a CT AGN at $z=3.7$ (Norman et al., 2002; Comastri et al., 2011). About 500 net counts are collected in 400 ksec (the exposure of the WFXT deep survey). The iron line is clearly detected and allows an accurate redshift determination.

merger rate alone, however, would simply increase the abundance of the *total* QSO population at high- z . It is the higher gas fraction that would produce a longer obscured phase at high- z and hence a higher fraction of obscured QSOs. If lower-luminosity objects are instead preferentially hosted by main sequence, non-interacting galaxies, the overall system geometry could be regular. Hence, a static geometry in the nuclear regions, as postulated in the classic Unified Models, could be valid and the observed obscuration would only depend on the line of sight. In this case, although a larger gas reservoir (higher f_{gas}) is available at high- z , the lack of interactions would keep it away from the BH: the available gas would then just be consumed to form stars. The system geometry will then be preserved in time and, in turn, the observed fraction of obscured AGN. This appealing scenario admittedly relies on a qualitative interpretation: further observations and detailed modeling are needed to test it in the next few years.

4. Prospects for the very near and mid-term future

Besides further analysis of Chandra and XMM data from completed (CDFS, COSMOS, AEGIS, XBootes) and on-going Ms sur-

veys (COSMOS-Legacy, XXL), a fundamental contribution to our understanding of hidden black holes is shortly expected by NuSTAR (Harrison et al., 2010), on orbit since June 2012. NuSTAR is carrying the first focusing optics at $E > 10$ keV and will overtake the sensitivity of current high-energy instruments by more than two orders of magnitude. The NuSTAR surveys in the CDFS and COSMOS fields will likely reach sensitivities of a few $\times 10^{-14}$ erg cm^{-2} s^{-1} in the 10-40 keV range. These appear obviously very shallow if compared with the Chandra or XMM data in the same fields. It is then unlikely that NuSTAR uncovers new X-ray sources in the CDFS and COSMOS, but high-energy data will significantly improve the N_H estimate for those already known. As far as the demography of CT AGN is concerned, the whole NuSTAR program is expected to detect Seyfert-like objects ($L_x < 10^{44}$ erg s^{-1}) up to $z < 0.5$ (in small numbers though), opening a new territory to test the assumptions of XRB synthesis models.

A real breakthrough in the study of the demographics of CT AGN would be possible in the next years if concept-missions like the Wide Field X-ray Telescope (WFXT; see Murray et al. this volume) will come into reality. WFXT would produce wide-and-deep surveys in the 0.5-7 keV band with an unprecedented grasp and *average* resolution across the field of view comparable to that of Chandra. Unlike standard Wolter-type mirrors, the polynomial mirrors design of WFXT is optimized to provide a constant PSF with off-axis angle, making this instrument a perfect survey machine. To give a sense of its capabilities, with its current survey strategy WFXT is expected to produce the equivalent of ~ 1000 CDFS surveys (at the 1Ms CDFS depth) *plus* 3000 C-COSMOS surveys. Based on the predictions of current XRB synthesis models, WFXT is expected to return \sim ten millions of AGN up to the highest redshifts ($z > 6$): about 5×10^5 AGN will be detected with more than 400 net counts, including 10^4 objects with $N_H > 10^{23}$ cm^{-2} , for which accurate X-ray spectra will be obtained. This spectral sample will allow an unambiguous determination of how unobscured and moderately obscured AGN evolve as a

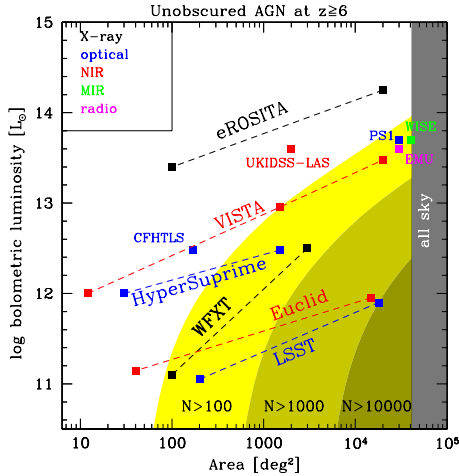


Fig. 5. Minimum bolometric luminosity of unobscured AGN at $z \geq 6$ detectable over a given survey area. Different colors refer to surveys in different wavebands (see upper-left corner). Shaded areas with progressively darker colors show the regions where a given survey should detect more than 100, 1000, and 10000 objects (assuming an exponential decline of the space density of AGN at $z > 3$; Brusa et al. 2009; Civano et al. 2011). WFTS matches in area and sensitivity future optical (HyperSuprime and LSST) and near-IR (Euclid) surveys.

function of redshift, luminosity, column density and environment, providing key information on BH/galaxy coevolution theories. In this sample, about 300 objects are expected to be *bona-fide* CT AGN at $z > 1$. As shown by the simulation in Fig.4, their WFTS spectra will reveal *directly* their CT nature, and measure their redshift through the detection of the iron $K\alpha$ feature. The cosmological evolution of the elusive CT AGN population will then be probed for the first time. Finally, WFTS is expected to detect > 1000 obscured and unobscured AGN at $z > 6$ (current model predictions vary by orders of magnitude), hence determining how the first black holes evolve: as shown in Fig.5, these data will perfectly match the other wide-and-deep multiwavelength survey data available in a 5-10 years time frame.

Acknowledgements. I wish to thank the members of the CDFS, COSMOS and WFTS collaborations for their help, and the organizers of the conference

“X-ray astronomy: towards the next 50 years” for their kind invitation. Support from ASI-INAF grant I/009/10/0 and PRIN-INAF 2011 is acknowledged.

References

- Akylas, A., et al. 2012, A&A, 546, A98
 Alexander, D. M., et al. 2011, ApJ, 738, 44
 Ballantyne, D. R., et al. 2006, ApJ, 639, 740
 Brusa, M., et al. 2009, ApJ, 693, 8
 Burlon, D., et al. 2011, ApJ, 728, 58
 Civano, F., et al. 2011, ApJ, 741, 91
 Comastri, A., et al. 2008, MmSAI, 79, 59
 Comastri, A., et al. 2011, A&A, 526, L9+
 Comastri, A., et al. 1995, A&A, 296, 1
 Elbaz, D., et al. 2011, A&A, 533, A119
 Elvis, M., et al. 2009, ApJS, 184, 158
 Feruglio, C., et al. 2011, ApJ, 729, L4+
 Fiore, F., et al. 2009, ApJ, 693, 447
 Georgantopoulos, I., et al. 2007, A&A, 466, 823
 Georgantopoulos, I., et al. 2011, A&A, 534, A23
 Giacconi, R., et al. 1962, Phys. Rev. Lett. 9, 439
 Gilli, R., et al. 1999, New Astronomy, 4, 45
 Gilli, R., et al. 2007, A&A, 463, 79
 Gilli, R., et al. 2010a, AIPC, 1248, 359
 Gilli, R., et al. 2011, ApJ, 730, L28
 Harrison, F. A., et al. 2010, SPIE, 7732
 Hasinger, G. 2008, A&A, 490, 905
 Hopkins, P. F., et al. 2008, ApJS, 175, 356
 Iwasawa, K., et al. 2012, A&A, 546, A84
 Kartaltepe, J. S., et al. 2012, ApJ, 757, 23
 La Franca, F., et al. 2005, ApJ, 635, 864
 Lilly, S. J., et al. 2007, ApJS, 172, 70
 Madau, P., et al. 1994, MNRAS, 270, L17
 Mignoli et al., M. 2013, A&A, submitted
 Moretti, A., et al. 2012, A&A, 548, A87
 Norman, C., et al. 2002, ApJ, 571, 218
 Pompilio, F., et al. 2000, A&A, 353, 440
 Rodighiero, G., et al. 2011, ApJ, 739, L40
 Rovilos, E., et al. 2012, A&A, 546, A58
 Setti, G. & Woltjer, L. 1989, A&A, 224, L21
 Tozzi, P., et al. 2006, A&A, 451, 457
 Treister, E., et al. 2012, ApJ, 758, L39
 Treister, E., et al. 2009, ApJ, 696, 110
 Tsujimoto, M., et al. 2011, A&A, 525, A25
 Ueda, Y., et al. 2003, ApJ, 598, 886
 Vignali, C., et al. 2010, MNRAS, 404, 48
 Vito, F., et al. 2013, MNRAS, 428, 354
 Wilman, R. J. et al. 1999, MNRAS, 309, 862
 Xue, Y. Q., et al. 2011, ApJS, 195, 10